THE CALCULATION OF SPACECRAFT POTENTIAL - COMPARISON BETWEEN THEORY AND OBSERVATION

H. B. Garrett
Air Force Geophysics Laboratory

SUMMARY

A simple charge balance model based on the work of DeForest has been adapted for the calculation of spacecraft potentials. The model is calibrated with ATS-5 plasma data from the University of California plasma experiments. Once calibrated, the model is used to calculate the time-varying potential that is observed as a spacecraft passes in and out of eclipse. Errors on the order of ±800 volts are observed over a range of 0 to -10,000 volts. Possible applications of the model to large space structures are discussed. Of special interest is the unique use of eclipse observations to test the spacecraft charging model.

INTRODUCTION

The calculation of the potential on a satellite immersed in a plasma is, at best, a difficult problem. In particular, the accurate prediction of the potential on a spacecraft in the space environment requires the simultaneous calculation of the paths of all charged particles in the vicinity of the spacecraft. In principle this is possible, in practice it is not feasible and a variety of techniques have been developed to simplify the problem (see, for example, Whipple, 1965 (ref. 1); Rothwell et al., 1977 (ref. 2); Laframboise and Prokopenko, 1977 (ref. 3); Parker, 1977 (ref. 4) and references therein). Although capable of an accurate treatment both in time and space, these models are limited in usefulness as they require large amounts of computer time or do not include all of the various current sources necessary to simulate the charging phenomenon. This paper describes an approximate solution to the problem that yields spacecraft potentials by making assumptions which are equivalent to the "thick sheath" probe solution for a sphere. Though similar models have been developed by Rosen (1975) (ref. 5); Massaro et al. (1977) (ref. 6); Inouye (1976) (ref. 7), and Purvis et al. (1977) (ref. 8), none have included the actual measured spectra in their calculations. The model to be described in this paper uses actual ATS-5 data and is adapted from methods originally developed by Whipple (1965) (ref. 1) and DeForest (1972) (ref. 9). The model, limited somewhat in its range of applicability to potentials of -10,000 volts and plasma temperatures between 50 eV and 30 keV, results in significant savings in computer time over more complicated models.

In the first part of this paper the model will be formulated. The individual current sources are presented and approximations as a function of satellite potential developed. The model is calibrated using actual ATS-5 observations of the potential. Two examples will be discussed in which the model is used to study the effects of the time-varying geosynchronous environment and of a time-varying photoelectron flux on spacecraft potential. Applications of the model will be briefly discussed.

MODEL FORMULATION

In solving the spacecraft charging problem, we are concerned with finding the spacecraft potential $\emptyset$ such that

$$J_e - (J_I + J_{se} + J_{sI} + J_{BSe} + J_{ph}) = 0 \qquad (1)$$

where J_e = Incident electron current

J_I = Incident ion current

J_{se} = Secondary emitted electron current due to J_e

J_{sI} = Secondary emitted electron current due to J_I

J_{BSe} = Back scattered electron current due to J_e

J_{ph} = Photoelectron emission

Given the incident ion and electron particle spectra, the currents J_e, J_I, J_{se}, J_{sI}, and J_{BSe} are found and adjusted by varying the potential on the spacecraft until equation (1) holds. This is the basic problem and in subsequent sections we will outline methods of calculating the currents as a function of potential.

ELECTRON AND ION INCIDENT CURRENT

The ATS-5 satellite employs electrostatic analyzers and, instead of the distribution function f (V) as a function of velocity V which is normally used in current calculations, these detectors return the differential energy flux, $\frac{d\,(EF)}{dE}$. Thus, it is convenient to express the integrals necessary to obtain the various currents in terms of the energy E and $\frac{d(EF)}{dE}$ rather than f(V) and V.

The conversion from f to $\frac{d(EF)}{dE}$ is given by

$$f = \frac{d\,(EF)}{dE} \quad \frac{\frac{1}{2}\,m^2}{E2} \tag{2}$$

where the conversion factors (K_e and K_I) are, if f is given in sec^3/km^6, $\frac{d(EF)}{dE}$ in $ergs/cm^2$ sec ster eV, and E in eV:

$$K_e = .1617 \text{ for electrons} \tag{3}$$

$$K_I = 5.45 \times 10^5 \text{ for ions} \tag{4}$$

As $\langle NF \rangle = \int_0^\infty V^3 f(V)\, dV$

This gives

$$\langle NF_e \rangle = K_e \int_0^\infty \frac{d(EF)}{dE}\bigg|_e \frac{dE}{E} \tag{5}$$

$$\langle NF_I \rangle = K_I \int_0^\infty \frac{d(EF)}{dE}\bigg|_I \frac{dE}{E}$$

where the results are left in terms of the number flux rather than actual current density J ($J = \pi q \langle NF \rangle$, where q is the charge on a particle). The values of $\frac{d(EF)}{dE}$ must be shifted by an energy equal to the desired potential before the integration (see Garrett, 1978 (ref. 10) for details). In the actual case an interpolation is necessary as the desired value of $\frac{d(EF)}{dE}$ for the shifted spectrum usually does not correspond to an observed value of $\frac{d(EF)}{dE}$. Further, as the ATS-5 data correspond to discrete energy bands for the range 51 eV to 51 keV, the integrals become sums (dE becomes ΔE) over this range. Results indicate that these approximations are adequate for a range of 50 eV to 30 keV in temperature and 0 V to -10,000 V in potential.

SECONDARY EMISSION CURRENTS

Electrons and ions striking the satellite surface are either scattered off the surface or cause the emission of low energy, secondary electrons.

Secondary emission is usually given in terms of the incident differential current density, $\frac{dJ_i}{dE}$. $\frac{dJ_i}{dE}$ is related to $\frac{d(EF)}{dE}$ by

$$\frac{dJ_i}{dE} = \frac{q\eta}{E} \frac{d(EF)}{dE} \tag{6}$$

(the $q\eta$ factor will be dropped in future discussions).

For secondary emission, the amount of secondary current emitted for a given incident flux is expressed as a ratio $\delta(E)$:

$$\delta(E) = \frac{dJ_s(E)}{dJ_i(E)} \tag{7}$$

where $\delta(E)$ = the secondary electron yield function

$\frac{dJ_s}{dE}$ = differential secondary current density

$\frac{dJ_i}{dE}$ = differential incident current density

From equations 6 and 7

$$\frac{d J_s(E)}{dE} = \delta(E) \frac{dJ_i}{dE}(E) = \frac{\delta(E)}{E} \frac{d(EF)}{dE} \tag{8}$$

The normalized differential current spectrum, $g(E')$, of the secondary electrons is approximately independent of the incident particle energy and, for aluminum, given in figure 1. Multiplying $g(E')$ by the secondary current density $J_s(E)$ gives the differential current density of secondary electrons due to particles of energy E as

$$\frac{dJ(E', E)}{dE'} = g(E') J_s(E) \tag{9}$$

This implies that the total current density is given by

$$J_{TS} = \int_0^\infty dE' \int_0^\infty dE \frac{d^2J(E', E)}{dE' dE}$$

$$= \int_0^\infty g(E')\, dE' \int_0^\infty \delta(E) \left[\frac{d(EF)}{dE}\right] \frac{dE}{E} \qquad (10)$$

$g(E')$ peaks sharply at ~ 2 eV and thus for ions and electrons is ~ 0 if the potential is greater than +2 volts (all the secondary electrons are attracted). Thus, to the order of accuracy of these calculations $g(E')\, dE'$ will be assumed = 0 for $\phi > 0$ and = 1 for $\phi \leq 0$. $\delta(E)$ is approximated for electrons impacting on aluminum by the curve shown in figure 2 (Whipple, 1965 (ref. 1)). $\delta(E)$ is not well known for ions impacting on aluminum but a fit to data as presented by Whipple (1965) (ref. 1)) for H^+ over the energy range of interest is presented in figure 3.

$\delta(E)$ for the incident ions and electrons is substituted into equation (10) and integrated using the appropriate shifted values for $\frac{d(EF)}{dE}$ to obtain the secondary emission currents due to the electrons and ions. Typically, the secondary emission due to electrons results in a current of approximately 25-50% that of the incident electron current while the secondary emission due to ions results in an electron current approximately 2-3 times that of the incident ions. As will be discussed shortly, it was necessary to adjust these values to obtain accurate estimates of the potential.

BACKSCATTERED ELECTRON CURRENT

Some incident electrons are reflected and give rise to the backscattered electron current (the backscattered current due to ions is very small and ignored). Although simple theories of collisional scattering such as those of Everhart (1960) (ref. 11) are useful in predicting the net current, experimental curves for backscattered emission from aluminum are also available. DeForest (1972) (ref. 9) has adapted the experimental results of Sternglass (1954) (ref. 12) to the ATS-5 data. His development, which will be presented here, is similar to that given for secondary electrons.

The basic equation for backscattering is

$$J_{BSe} = \int_0^\infty dE' \int_{E'}^\infty B(E', E) \frac{dJ_i(E)}{dE} dE \qquad (11)$$

where E' = energy of backscattered particles ($E' \leq E$)

E = energy of incident particles

$B(E',E)$ = percentage of electrons scattered at a given energy E' as a result of an incident electron at energy E

$J_i(E)$ = incident current (electrons in this case)

From Sternglass (1954) (ref. 12)

$$B(E',E) = \frac{G(E'/E)}{E} \tag{12}$$

G is given as a function of $K = E'/E$ (DeForest, private communication) in figure 4 for aluminum.

Continuing, equation 11 becomes

$$J_{BSe} = \int_0^{\infty} \frac{dE'}{E'} \int_{E'}^{\infty} \left[\frac{E'}{E} G\left(\frac{E'}{E}\right)\right] \left.\frac{d(EF)}{dE}\right|_e \frac{dE}{E} \tag{13}$$

Substituting the proper values of $\left.\frac{d(EF)}{dE}\right|_e$ in equation (13) and performing the integration gives the total current due to backscattered electrons. For aluminum, a ratio of ~25% for the backscattered current to incident current is obtained in agreement with other estimates. Unlike the secondary electron current, though, the backscattered current is a gradual function of positive spacecraft potential. For positive potentials, the 0 integral limit in equation (13) is replaced by $|q\phi|$, the energy shift due to the spacecraft potential.

PHOTOELECTRON EMISSION

Light, particularly in the ultraviolet, falling on the spacecraft causes the emission of photoelectrons. Although the characteristics of the emitted particles and the processes involved are well known, the actual photoelectron emission from a spacecraft is poorly known. The reason is the variety of materials on the typical spacecraft surface and the lack of precise knowledge of the solar spectrum and its interaction with various materials. Grard et al. (1973) (ref. 13) and Whipple (1965) (ref. 1) have combined the solar spectrum with the emission characteristics of various substances to give the photo-

electron current as a function of energy. DeForest (private communication) has developed an algorithm that approximates their results. It gives the photoelectron current as a function of positive spacecraft potential (for negative potential all of the photoelectron current leaves the spacecraft). It is

$$J_{ph} = \frac{J_{po}}{(\phi/.7+1)^4} \tag{14}$$

Values for J_{po} are given in Table 1. From this table it is clear that estimates of J_{po} range over an order of magnitude. Fortunately, most examples of charging that we will be concerned with involve shadowed surfaces, in which case $J_{po} = 0$. The charging model will, however, in conjunction with actual data, be used in a later section to estimate the value of J_{po} appropriate to ATS-5.

COMPARISON WITH DATA

The ultimate check of any model is how well the predicted results compare with actual measurements. The basic set of data will be spectra from ATS-5 for periods immediately before and after entry into the earth's shadow. These periods were selected as they can be used not only to study large potential variations (on the order of ~6 keV) but also to calibrate the photoelectron flux. Table 2 lists the eclipses studied and the potentials observed during the eclipses.

ATS-5 does not consist of a single material nor can it be said to be spherical in shape (a tacit assumption in the preceding analysis). However, keeping to the spirit of a "simple" charging model, the satellite was approximated as an aluminum sphere. Figure 5 shows the results of these calculations. The discrepancies between observed and predicted potentials have been corrected by adjusting the magnitudes of the secondary emission terms by multiplying each one by a constant correction factor to give a best fit in a least squares sense (the backscattered flux is directly proportional to the incident electron flux so that determining its coefficient is somewhat difficult as it may reflect slight errors in the actual measurement of J_e). For correction factors of 1.3 (J_{se}), .55 (J_{sI}), and .4 (J_{BSe}), the results have a standard deviation of +800 volts. It should be kept in mind, though, that the model is based on several assumptions and, considering these, this agreement is quite good.

MODEL APPLICATION

The model has been developed for two purposes. First, combined with the geosynchronous plasma model developed by Garrett (1977) (ref. 14), it can be used to predict potentials on spacecraft as a function of the geomagnetic index

A_p and LT, the satellite local time. It also is employed to calculate the potential on a spacecraft as it passes into and out of the earth's shadow.

Figure 6 plots the potential variations predicted by the model for the geosynchronous simulation model of Garrett (ref. 14) (1977) for moderate geomagnetic activity (A_p = 15) and high geomagnetic activity (A_p = 207). That simulation gives a "2 Maxwellian fit" to the plasma such that the distribution functions are for electrons

$$f_e(E) = 27.2\left[N_e \left(\frac{T1_e}{1000}\right)^{-3/2} e^{-E/T1_e} + N2_e \left(\frac{T2_e}{1000}\right)^{-3/2} e^{-E/T2_e} \right] \quad (15)$$

and for ions

$$f_I(E) = 2.14\times10^6\left[N1_I \left(\frac{T1_I}{1000}\right)^{-3/2} e^{-E/T1_I} + N^2{}_I \left(\frac{T2_I}{1000}\right)^{-3/2} e^{-E/T2_I} \right] \quad (16)$$

where $N1_e$, $N2_e$ = electron number densities (n/cm^3)

$T1_e$, $T2_e$ = electron temperatures (eV)

$N1_I$, $N2_I$ = ion number densities (n/cm^3)

$T1_I$, $T2_I$ = ion temperatures (eV)

The distribution functions are converted to differential energy spectra using equation (2). The spectra are inserted into the program and, assuming no photoelectron current, the potential calculated. These potentials are the maximum that would be expected for a shadowed, electrically isolated surface as a result of the ambient environment.

Another use of the model is in the determination of the potential as a spacecraft passes into the earth's shadow. The eclipse data described earlier are used in conjunction with the model to determine the current necessary to give the observed potential variations as ATS-5 passed into and out of the

earth's shadow. Presumably, this residual current is the photoelectron current. By varying the amplitude of an appropriate model of atmospheric attenuation to fit this residual (or photoelectron) current, J_{po} was found. The results for ATS-5 for 2 atmospheric models are illustrated in figure 7. The resulting J_{po} value was determined to be .4 n Amps/cm^2 for the best atmospheric model which is in agreement with the lower values in Table 2. The reader is referred to Garrett (1978) (ref. 15) for details of this procedure.

Figure 8 shows the observed and predicted potentials as ATS-5 passes into and out of eclipse on days 260 and 292, 1970. In figure 9 are similar results for ATS-6 on days 59 and 66, 1976. The results of the predictions are adequate and within the $\pm$800 V error but their deviations from the observed values at low potential may indicate either a need to include sheath effects or that the thick sheath, spherical probe approximation is inaccurate for low ($\lesssim$ 100 V) potentials. In any event, this method of testing, by comparing the observed and predicted potentials as the photoelectron flux is varied, should prove to be a powerful tool for comparison with other spacecraft charging models in the future.

Given that the model is valid, it can be employed in a variety of simulations. Considering that a photoelectron current is in most physical respects identical with an electron beam, the model can test the effects of charged beams on satellites. Likewise, the data employed in calibrating the model can be used to test other models of beam phenomena. Although the scaling of our results to large structures may be somewhat dubious quantitatively, it is clear that the model can also estimate possible effects on large structures. For example, if we approximate a large structure by nodes which must meet equation (1), then the model can be used to predict the potential at each point on the surface of a large structure as it enters eclipse. When this is done, it turns out that rather large time varying potential gradients due solely to different photoelectron emission rates on a structure can be generated - a clear threat to future missions.

CONCLUSION

A simple model based on the work of Whipple (1965) (ref. 1) and DeForest (1972) (ref. 9) has been developed. The model was calibrated with ATS-5 plasma data. The model predictions for the potential on a satellite as it passed into eclipse were compared with actual observations. The results indicate agreement between the predicted and observed values. The model is used in conjunction with a model simulation of the geosynchronous environment to predict spacecraft potentials under different geomagnetic and local time conditions. The model, after being calibrated, successfully predicts potentials with $\pm$800 V accuracy over a range of 10,000 V. It includes relevant current terms and is efficient in comparison with other complex models taking $\sim$2 sec per potential calculation. FORTRAN programs are available from AFGL.

REFERENCES

1. Whipple, E. C. (1965): The Equilibrium Electric Potential of a Body in the Upper Atmosphere, NASA X-615-65-296.

2. Rothwell, P. L., Rubin, A. G., and Yates, G. K. (1977): A Simulation Model of Time-Dependent Plasma-Spacecraft Interactions, Proc. of the Spacecraft Charging Conference, AFGL-TR-77-0051/NASA TMX-73537.

3. Laframboise, J. G., and Prokopenko, S.M.L. (1977): Numerical Simulation of Spacecraft Charging Phenomena, Proc. of the Spacecraft Charging Conference, AFGL-TR-77-0051/NASA TMX-73537.

4. Parker, L. W. (1977): Calculation of a Sheath and Wake Structure About a Pill Box-Shaped Spacecraft in a Flowing Plasma, Proc. of the Spacecraft Charging Conference, AFGL-TR-77-0051/NASA TMX-73537.

5. Rosen, A. (1975): Spacecraft Charging: Environment Induced Anomalies, Paper 75-91, AIAA 13th Aerospace Sciences Meeting, 1975.

6. Massaro, M. J., Green, T., and Ling, D. (1977): A Charging Model for Three-Axis Stabilized Spacecraft, Proc. of the Spacecraft Charging Conference, AFGL-TR-77-0051/NASA TMX-73537.

7. Inouye, G. T. (1976): Spacecraft Potentials in a Substorm Environment, Spacecraft Charging by Magnetospheric Plasma, AIAA Progress in Astronautics and Aeronautics Series, Vol 42, Rosen (Editor).

8. Purvis, C. K., Stevens, N. J., and Oglebay, J. C. (1977): Charging Characteristics of Materials: Comparison of Experimental Results with Simple Analytical Models, Proc. of the Spacecraft Charging Conference, AFGL-TR-77-0051/NASA TMX-73537.

9. DeForest, S. E. (1972): Spacecraft Charging at Synchronous Orbit, J. Geophys. Res., 77: (No. 4): 651.

10. Garrett, H. B. (1978): Spacecraft Potential Calculations - A Model, AFGL-TR-78-0116.

11. Everhart, T. E. (1960): Simple Theory Concerning the Reflection of Electrons from Solids, Journal of Appl. Phys., 31: (No. 8): 1483.

12. Sternglass, E. J. (1954): Backscattering of Kilovolt Electrons from Solids, Phys. Rev., 95: 345.

13. Grard, R.J.L., Knott, K. and Pedersen, A. (1973): The Influence of Photoelectron and Secondary Electron Emission on Electric Field Measurements in the Magnetosphere and Solar Wind, Photon and Particle Interactions with Surfaces in Space, R.J.C. Grard (Ed.) D. Reidel Publishing Co., Dordrecht, Holland, pp.163-189.

14. Garrett, H.B. (1977): Modeling of the Geosynchronous Orbit Plasma Environment, Part I, AFGL-TR-77-0288.

15. Garrett, H.B. (1978): Effects of a Time-Varying Photoelectron Flux on Spacecraft Potential, AFGL-TR-78-0119.

TABLE 1

Author	Saturation Current (n Amps/cm^2)	
Grard et al. (1973)[13]	4.20	(Aluminum oxide)
	3.00	(Indium oxide)
	.40	(Graphite)
DeForest (1972)[9]	.82	(ATS-5)
Whipple (1965)[1]	3.00	(Rocket-aluminum)

TABLE 2

Date	UT	Potential
1969 22 Sep	0629	-3400
	0731	-3810
16 Oct	0627	-5360
	0711	-3810
1970 12 Sep	0631	-2420
	0718	-1730
15 Sep	0626	-877
	0721	-1540
17 Sep	0623	-5380
	0723	-3040
19 Sep	0620	-2720
	0724	-1940
26 Sep	0724	-2170
17 Oct	0630	-1230
	0659	-2170
18 Oct	0633	-397
	0650	-316
19 Oct	0640	-396
	0648	-558

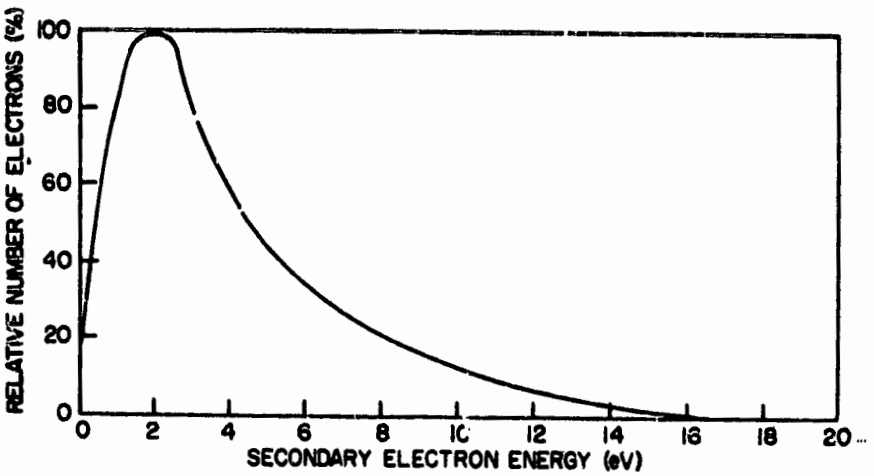

Figure 1. - Relative number of emitted secondary electrons as function of energy. (From Whipple (1965), ref. 1.)

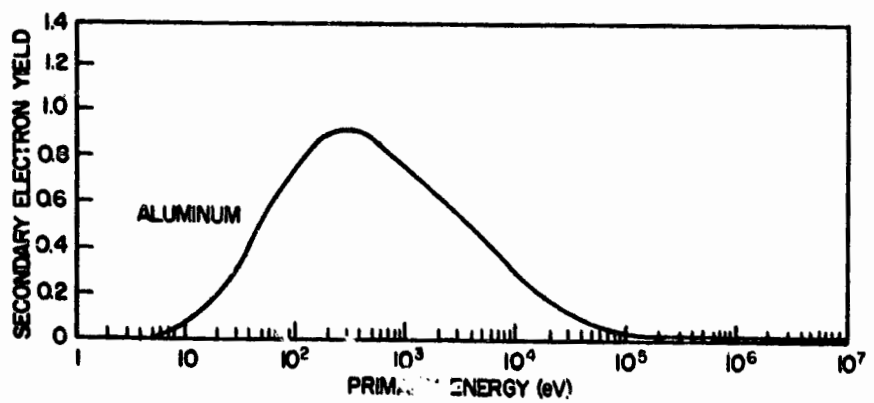

Figure 2. - Secondary electron yield for electron impact on aluminum as function of energy. (From Whipple (1965), ref. 1.)

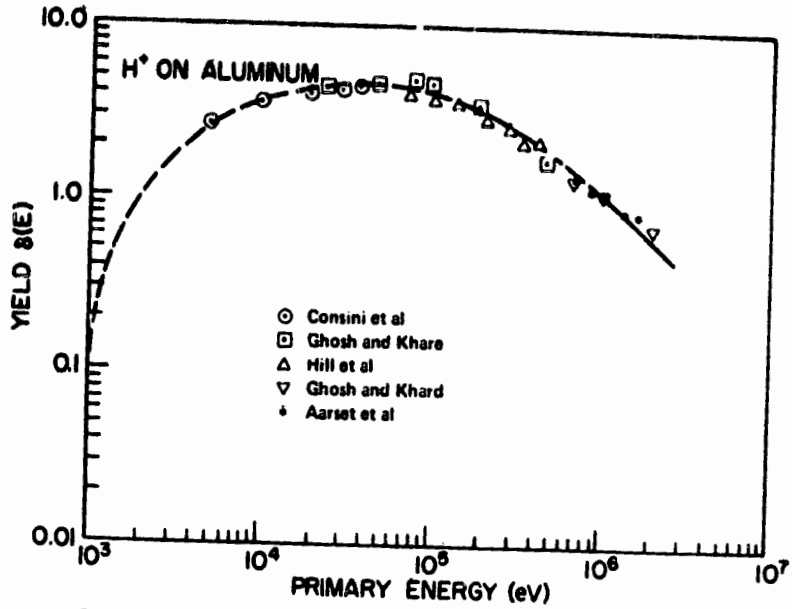

Figure 3. - Secondary electron yield for ion (H^+) impact on aluminum as function of energy. (From Whipple (1965), ref. 1.)

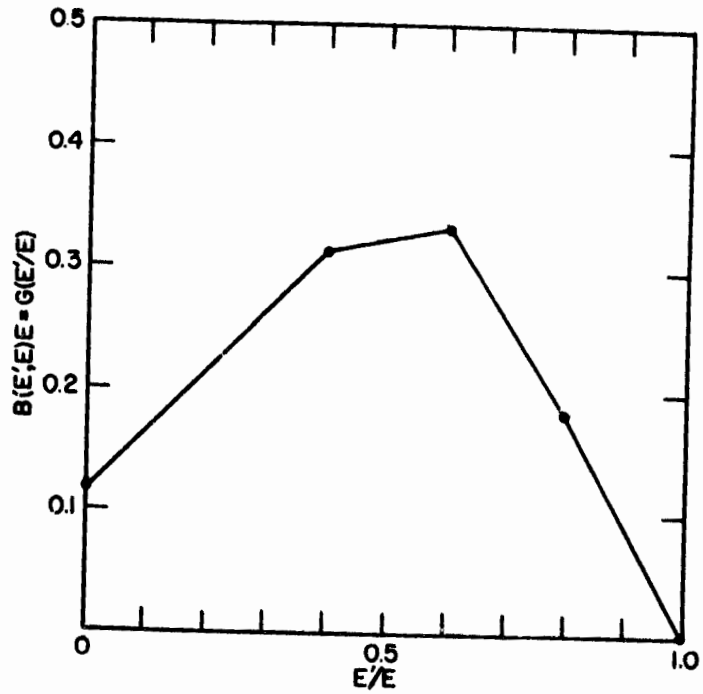

Figure 4. - B(E', E) · E as function of (E'/E) where B(E', E) is approximately the percentage of electrons scattered at a given energy E' as a result of a particle at an incident energy E. (From Sternglass (1954), ref. 12.)

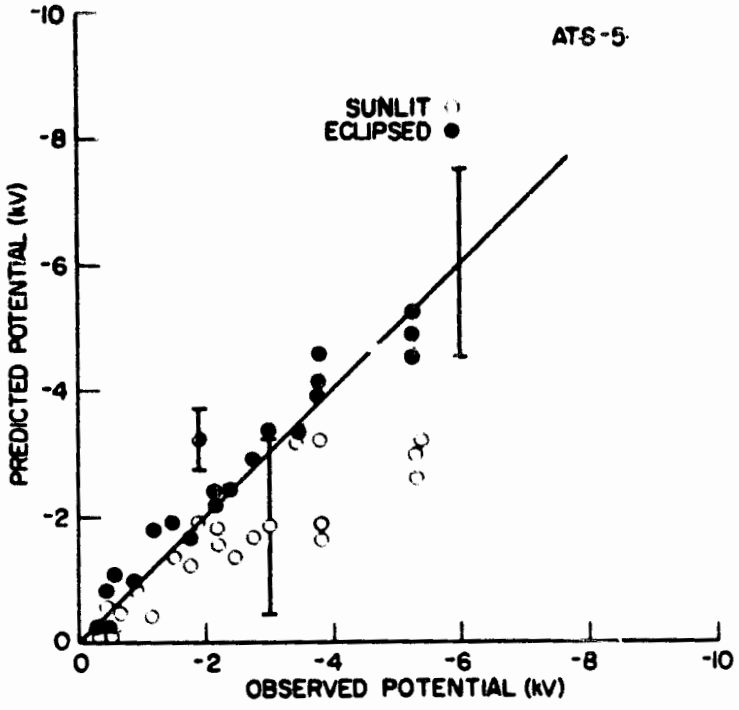

Figure 5. - Predicted potential as function of observed potential. (Results are for spectra when satellite was illuminated (sunlit) and when it was shadowed (eclipsed).)

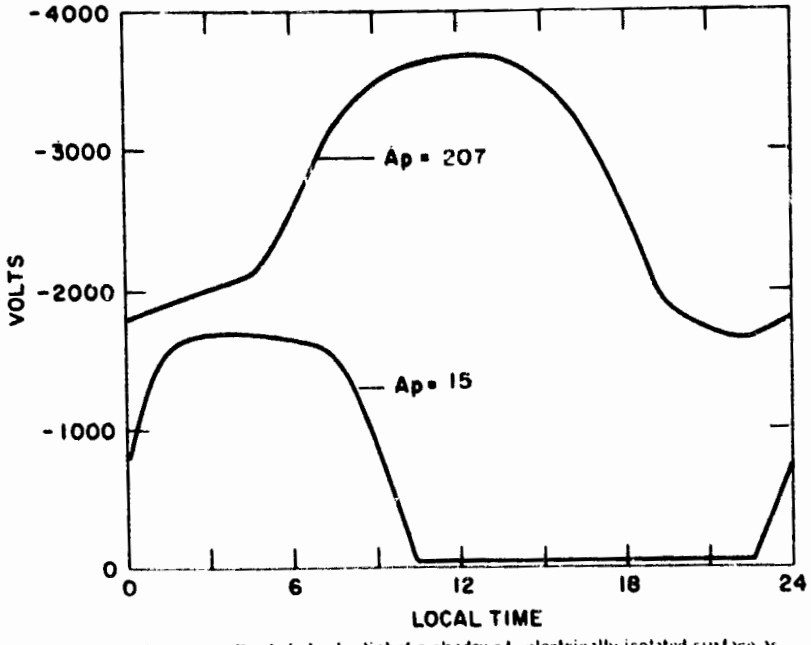

Figure 6. - Predicted potential of a shadowed, electrically isolated surface as function of time.

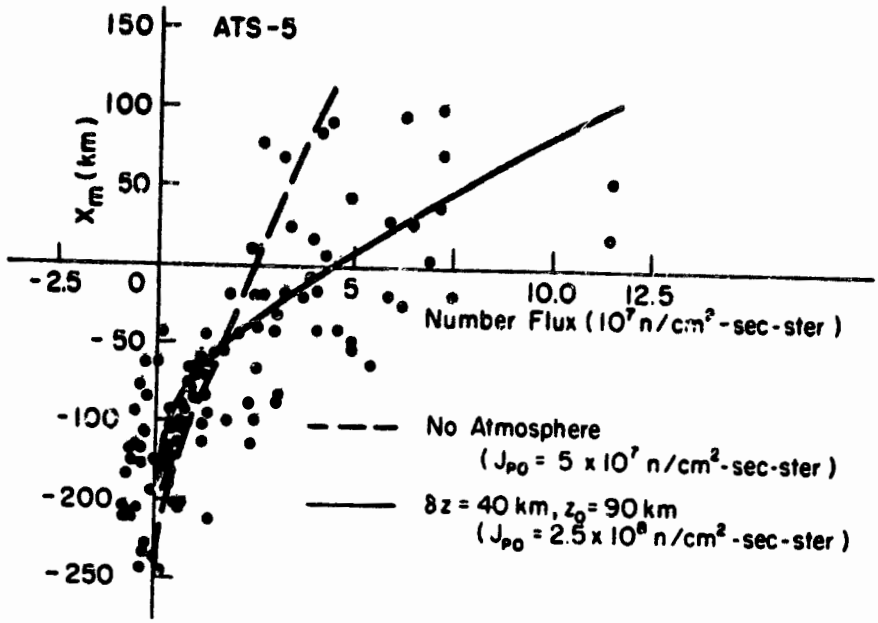

Figure 7. - Residual (photoelectron) current estimated for 21 ATS-5 eclipse passages. (This is the current necessary to explain the observed satellite potential after all ambient and secondary currents have been substracted. Two atmospheric attenuation profiles are also plotted.)

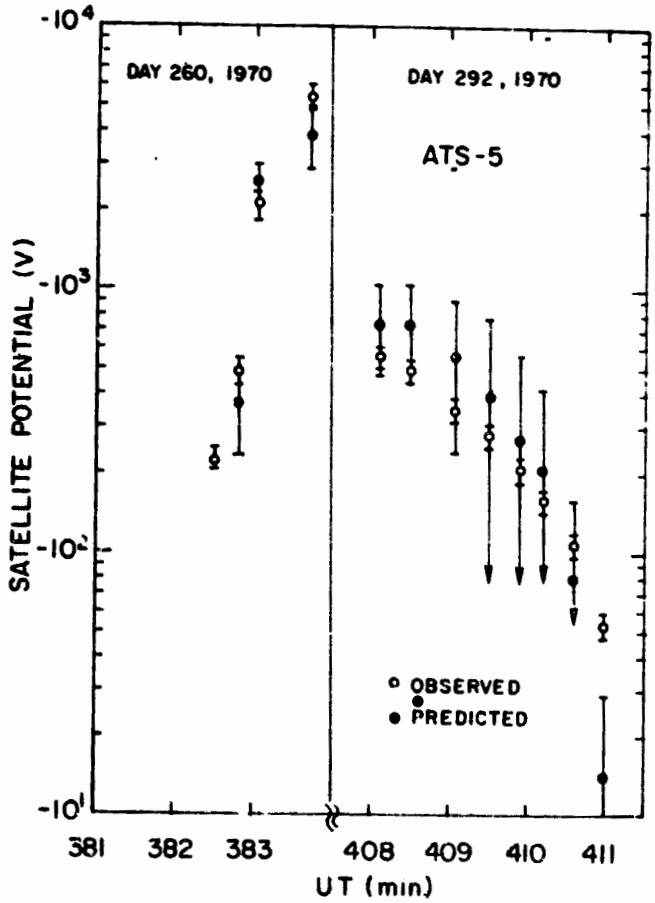

Figure 8. - Observed and predicted (average of sunlit and eclipsed spectra) potentials for eclipse entry of ATS-5 on day 260, 1970, and for eclipse exit on day 292, 1970.

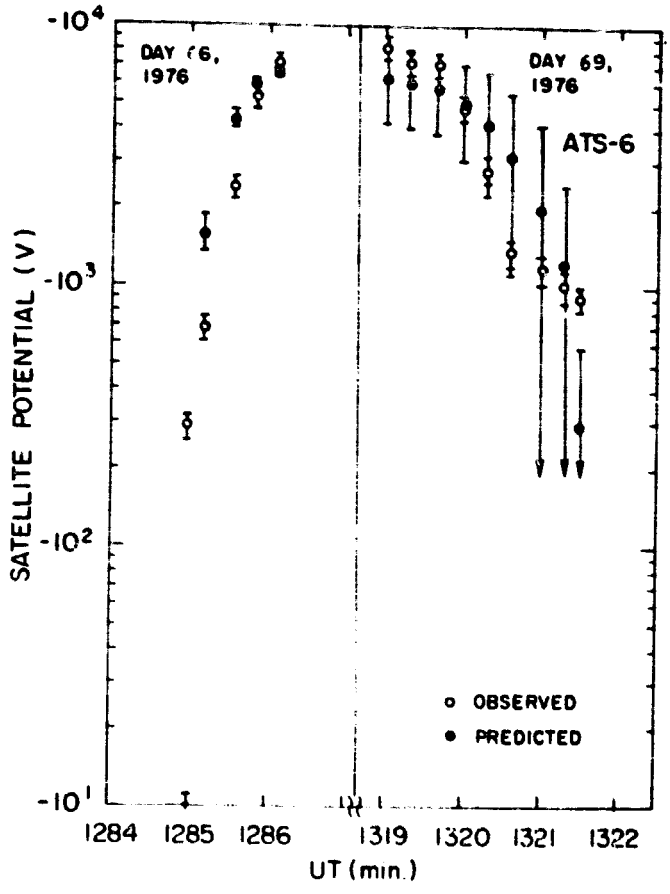

Figure 9. - Observed and predicted (average of sunlit and eclipsed spectral potentials for eclipse entry of ATS-6 on day 66, 1976, and eclipse exit on day 69, 1976.